DOE SBIR Phase I Final Report

Performing Organization:
Actoprobe LLC
801 University S.E., Suite 100,
Albuquerque, New Mexico, 87106

September, 4th, 2016

Authors: Gennady Smolyakov, Fei-Hung Chu, Chih-Feng Wang, Chengao Wang, Dmitri Tenne, Jeffrey J. Rack, Kevin Malloy and Alexander Ukhanov

Reporting Period: 02/22/2016 – 08/21/2016

SBIR Phase I Project Title: Atomic Force Microscope Active Optical Probe for Single-Molecule Imaging and Time-Resolved Optical Spectroscopy

DOE Grant Number: DE-SC0015188

Funding Office: Office of Science, U.S. Department of Energy

Abstract

Actoprobe LLC is reporting on the results of its DOE SBIR Phase I project for the development of Atomic Force Microscope Active Optical Probe for Single-Molecule Imaging and Time-Resolved Optical Spectroscopy. While chemistry, science, and technology greatly benefit from Atomic Force Microscopy in surface characterization, time-resolved chemical imaging on the single-molecule level lags far behind. Current scanning probe microscopy only obtains information about mechanical, but not optical/chemical properties. In order to address this problem, the Actoprobe LLC research team has proposed a novel class of Atomic Force Microscopy probes, Ultra-Fast Pulsed Active Atomic Force Microscopy Optical Probes (UFP AAOP), that will allow ultrafast time-resolved optical and chemical imaging at the nanoscale. As envisioned, these unique optical probes will perform the functions of conventional Atomic Force Microscopy probes and, in addition, will simultaneously provide chemical information about molecular scale interactions. This innovation is accomplished by integrating an ultra-fast pulsed laser source into an Atomic Force Microscopy probe. This report describes our progress with fabrication of an ultrafast micrometer-size semiconductor laser integrated with an Atomic Force Microscopy probe. In this Phase I project, we have demonstrated the feasibility of the UFP AAOP concept, and have fabricated a first prototype of the UFP AAOP. Excellent performance of the probe has been proven in terms of AFM and optical spatial resolution through rigorous

tests. The observed 20-nm optical resolution implies the potential capability for the probe to characterize chemical compounds with single-molecule resolution. We have shown that passive mode-locking operation provides short optical pulses at a repetition rate of 7.4 GHz with duration of ~17 ps, which makes it very attractive for time-resolved optical spectroscopy. The UFP AAOP fabrication procedure has been developed for wafer-scale production of multiple devices, with the yield of the process estimated to be ~90%. We have identified the particular photochromic compounds to be very good candidates for future testing of UFP AAOP time-resolved capability (Pulsed Tip-Enhanced Raman Spectroscopy). We have demonstrated the applicability of Raman Spectroscopy for studying the dynamics of photochromic reactions in diarylethene molecules by showing the differences in Raman spectra recorded before and after isomerization. Finally, economic feasibility and scale-up manufacturing potential was analyzed for UFP AAOP and found to be very promising. In summary, the Actoprobe team has successfully accomplished all of its Phase I tasks and demonstrated the feasibility of the UFP AAOP concept. We believe that this success provides a strong foundation for development in the Phase II project.

Table of Contents

List of Figures

List of Tables

Summary

The current commercially available system for nanoscale characterization is not only very expensive and complex, but also does not provide time-resolved information. Attempts to monolithically integrate AFM and active optical components have proven to be challenging and have only found limited applications due to low output power. Ultrafast TERS measurement is an important technique to monitor chemical reactions but has proved to be difficult and has not been commercialized yet. Therefore, it is of great interest to have a cost-effective solution for combined AFM/NSOM/TERS system with time-resolved data.

Actoprobe LLC proposed to develop and commercialize a novel class of probes–Ultrafast Pulsed Active AFM Optical Probe (UFP AAOP)—that will perform the functions of conventional AFM probes and simultaneously provide information about **chemical properties** of the specimen at the nanoscale together with time-resolved spectroscopy. This innovation will be accomplished by integrating a UFP laser source monolithically into an AFM probe.

UFP AAOP has significant potential to outperform current instruments in data quality and ease of operation and this enhanced functionality is expected to provide 5- to 10-times lower cost than that of a dedicated NSOM or TERS instrument.

This imaging technique combining molecular scale spatial resolution and ultrafast temporal resolution can be applied for exploring energy flow, molecular dynamics, breakage/formation of chemical bonds or conformational changes in nanoscale systems. One example of the application of pulsed TERS is to study the ultrafast dynamics of the photochromic reactions in diarylethene molecules, which is discussed later in this report.

As a result of the Phase I project, we have demonstrated the feasibility of the UFP AAOP concept. We have successfully fabricated an active optical AFM probe that incorporates passive mode-locked GaAs-based diode laser and GaAs AFM probe. Excellent performance of the probe has been proven in terms of AFM and optical spatial resolution through rigorous tests. The observed 20-nm optical resolution implies the potential capability for the probe to characterize chemical compounds with single-molecule resolution. Unique spatial information has been obtained from the near-field images, which implies very interesting potential applications of the probe for IR sensor characterization and development. Passive mode-locking operation was demonstrated and characterized for a two-section quantum dot laser designed for integration with GaAs AFM probe. We have shown that passive mode-locking operation provides short optical pulses at a repetition rate of 7.4 GHz with duration of ~17 ps, which makes it very attractive for time-resolved optical spectroscopy. Mode-locked diode laser and AFM optical probe was monolithically integrated into a single device – UFP AAOP. The UFP AAOP fabrication procedure has been developed for wafer scale production of multiple devices, with the yield of the process estimated to be ~90%. We have identified the particular photochromic compounds to be very good candidates for future testing of UFP AAOP time-resolved capability (pulsed TERS). We have demonstrated the applicability of Raman for studying the dynamics of photochromic reactions in diarylethene molecules by showing the differences in Raman spectra recorded before and after isomerization. UFP AAOP is expected to ensure single-molecule resolution for such measurements. Finally, Actoprobe analyzed the economic feasibility and scale-up manufacturing potential for the UFP AAOP, with very promising results.

In conclusion, we have accomplished all objectives and successfully completed all major tasks of

the project. We are excited about moving this project to Phase II to successfully commercialize the product. More effort and funding is needed to lower the cost of the fabrication process and scale up manufacturing capabilities. This technique also needs to be tested for more unique applications (niche markets) to investigate additional fields and target more future markets.

Introduction

The next big advance in nanotechnology research is likely to come from a more comprehensive understanding of processes and effects at the molecular or even the chemical bond level. These types of studies are highly dependent on microscopy/spectroscopy equipment capable of detecting single molecules. The current commercially available state-of-the-art microscopy/spectroscopy tool is a hybrid system combining Atomic Force Microscopy (AFM), Near-field Scanning Optical Microscopy (NSOM) and optical spectroscopy such as Tip-Enhanced Raman Spectroscopy (TERS) [1]. This equipment is expensive and complex, preventing widespread adoption in science and industry, and it does not provide time-resolved data.

Commercial products have also been developed based on techniques that integrate AFM and active optical components. AFM tips with integrated waveguides (hollow tips) are used in conjunction with an external laser source [2]. This high-cost approach suffers from inherent limitations of optical resolution and delivered light power. For high lateral resolution, the size of the near-field aperture needs to be reduced, leading to an exponential decrease of optical power output. This approach has limited application for near-field microscopy with ultimate resolution of about 50 nm, but is not appropriate for optical spectroscopy because of low power output.

Other approaches aimed at better integration of a light source and AFM tip have generally involved either a) attaching a prefabricated light source (edge emitter, VCSEL, or LED) above a Si AFM cantilever probe (hybrid approach) [3] or b) fabrication of the light source directly on the AFM tip [4]. In these instances, the optical detectors were not integrated into the probes. The hybrid approach has only been shown to work in research labs. Cost-effective fabrication of those optical probes to make them affordable for a wider scientific community is problematic. In addition, VCSELs, commonly used in this approach, are limited in their optical output power.

Single, integrated photodetectors have also been fabricated on AFM tips [5]. The photodetector-only approach [5] does not address the difficulties of aligning the light source to the AFM tip, and the requirement to reduce detector size to achieve spatial resolution directly contradicts the requirement to have the largest possible detection area necessary to obtain high sensitivity levels for optical spectroscopy on nanoscale.

In the past 30 years, the Raman scattering technique has been established as the most sensitive probe of chemical composition, with many advances demonstrated in the development of spontaneous Raman (conventional, most widely used), surface-enhanced, and nonlinear Raman techniques. There has been significant progress in ultrafast nonlinear stimulated Raman spectroscopy (SRS) using ultrashort laser pulses [6, 7]. Being a useful technique for observing molecular dynamics, SRS, however, is very limited in terms of chemical specificity. The narrow-band pump and Stokes excitation fields interact with a single molecular vibration, and the overlapping Raman bands cannot be distinguished. Very often, a priori knowledge of the chemical content and specific molecular vibration spectrum is required. Spontaneous Raman spectroscopy, on the other hand, offers a much more distinct fingerprint for convenient chemical identification, but is much less advanced in terms of ultrafast pulsed spectroscopy. In the context of conventional spontaneous Raman, ultrafast pulsed spectroscopy is normally employed for fluorescence background rejection, based on different time scales for the fluorescence and Raman scattering processes [8, 9]. The very first attempts have recently been reported at making

ultrafast spectroscopy with TERS [10, 11]. Demonstrating TERS with a pulsed excitation source is considered to be a very important step toward monitoring chemical reactions on the pico- to femtosecond time scale with the high spatial resolution and chemical specificity. Nevertheless, integration of an external pulsed excitation source (typically Ti:sapphire laser) is very challenging [11].

In short, the current commercially available system for nanoscale characterization is not only expensive and complex, but also does not provide time-resolved information. Attempts to monolithically integrate AFM and active optical components has been proved to be challenging and has found only limited applications due to low output power. Ultrafast TERS measurement is an important technique to monitor chemical reactions but proved to be difficult and has not been commercialized yet. Therefore, it is of great interest to have a cost-effective solution for combined AFM/NSOM/TERS system with time resolved data.

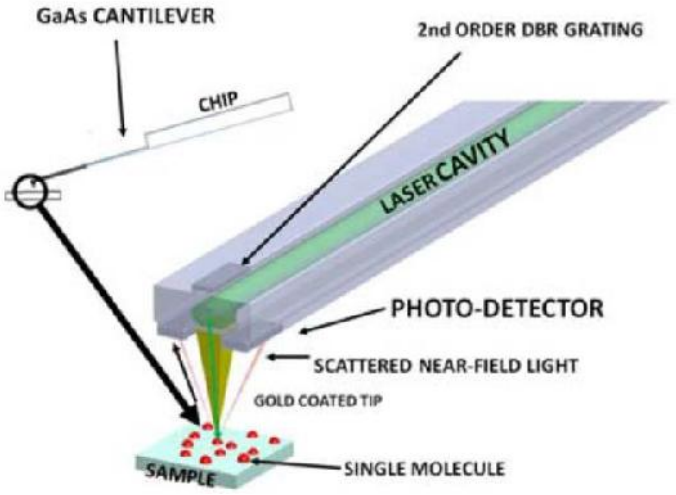

Fig.1. 3-D illustration of the UFP AAOP concept.

Actoprobe LLC proposed to develop and commercialize a novel class of probes for Scanning Probe Microscopy (SPM) – Ultrafast Pulsed Active AFM Optical Probe (UFP AAOP) that will **enhance characterization capabilities at the nanoscale**. These unique optical probes will perform the functions of conventional AFM probes and simultaneously provide information about **chemical properties** of the specimen at the nanoscale together with time-resolved spectroscopy. This innovation will be accomplished by integrating a UFP laser source and a photodetector monolithically into an AFM probe (Fig.1).

We believe this **enhanced functionality** can be achieved at **5- to 10-times lower cost than** that of a dedicated NSOM or TERS instrument. Moreover, our optical probes have **significant potential to outperform those instruments in data quality and ease of operation.** To meet all these requirements, we will fabricate a monolithic, integrated optical AFM probe from commercially available GaAs-based semiconductor diode laser wafers. Edge-emitting laser diodes, light guides, and efficient photodetectors will be fabricated by patterning the active region (epi-layer), while the AFM tip will be made from the GaAs substrate at the end of a cantilever formed from the epi-layers of the laser structure. This process avoids hybridization

and should allow for high-volume manufacturing, resulting in a cost-effective, affordable product that can be adopted for use by all current owners of AFMs.

The most widely used AFM probes are fabricated using silicon technology. In contrast, our UFP AAOPs are fabricated from GaAs, a semiconductor material suitable for optoelectronic device fabrication. The laser and detector functionality is enabled by an epitaxially grown structure that can be obtained commercially. The choice of GaAsis is motivated by the large base of established fabrication technologies, which allows time- and cost-effective fabrication of the probes. In the future, other III-V semiconductors, such as InP, GaP, GaSb, and GaN could be used to expand the available wavelength coverage from the UV to visible and mid-infrared. The advantage of this novel probe over NSOM is also determined by the high refractive index of GaAs. The UFP AAOP is operated with an aperture large enough, so that the wavelength is just below the waveguide cut-off. Since NSOM uses glass with a lower refractive index, it has significantly shorter cut-off wavelength and cannot work efficiently in near-infrared (NIR) spectral range. the high refractive index of GaAs translates into a dramatic increase of several orders of magnitude in transmission through the same size aperture and leads to high signal-to-noise ratio and high sensitivity of UFP AAOP in NIR.

The UFP AAOP can also be operated apertureless using surface plasmons, as an optical antenna [12]. TERS works similarly, but its performance is challenged by scattered light from the far field, leading to a large background signal. The apertureless UFP AAOP operated in surface plasmon mode will possess all the advantages of TERS. In addition, for the UFP AAOP, the light is supplied through the tip; hence, there is no scattered far-field light and thus significantly reduced background. Furthermore, the difficulties associated with laser alignment onto the tip and with imaging the signal onto a detector are avoided with the UFP AAOP.

Actoprobe is in an ideal position to advance this technology further by monolithically integrating a passively mode-locked pulsed semiconductor laser source into AFM probes, providing additional advantages to the scheme of ultrafast pulsed TERS. We believe our approach will lead to dramatically reduced background and automatic focusing of the excitation light to the probe tip. The active probe will supply sufficient optical power for performing two-photon-induced fluorescence in the visible optical range at the nanoscale. Ultrafast light pulses generated in the near field within a few nanometers distance of the tip will be free of any distortion normally associated with pulse propagation through focusing optics, and thus there will be no need for chirp compensation. The technology of mode-locked semiconductor lasers for ultrafast optical pulse generation is very well established for various gain media. The best results in terms of pulse duration have been obtained from Quantum Dot (QD) semiconductor lasers [13]. Pulses as short as 390 fs have been reported in two-section passively mode-locked QD lasers [14]. The very first to come up with the demonstration of passive mode-locking in QD lasers was the research group of Dr. Kevin Malloy [15], who is a consultant on this Project.

Integrating the ultrafast pulsed laser source into GaAs AFM probe will allow probing the site-specific dynamic response of chemical systems. This imaging technique combining molecular scale spatial resolution and ultrafast temporal resolution can be applied for exploring energy flow, molecular dynamics, breakage/formation of chemical bonds or conformational changes in nanoscale systems. One example of the application of pulsed TERS is to study the ultrafast dynamics of the photochromic reactions in diarylethene molecules, which is discussed later in this report.

Besides ultrafast pulsed TERS, the UFP AAOP technology can be modified to realize SRS or ultrafast pump-probe spectroscopy techniques by adding a second external laser source for pump field that can be harmonically synchronized [16] with the internal mode-locked laser source of probe/Stokes field. The tip-enhanced capability of UFP AAOP will allow single-molecule resolution, currently not attainable in SRS [7] or confocal ultrafast pump-probe spectroscopy [17].

Phase I Technical Objectives

The overall goal of the Phase I project is to prove the feasibility of developing, validating, and commercializing an AFM active optical probe with a monolithically integrated mode-locked semiconductor laser for nano-imaging and time-resolved spectroscopy.

The specific technical objectives for the Phase I project are as follows:

Objective 1. Demonstrate the technical feasibility of the AFM Active Optical Probe for ultrafast spectroscopy. The critical step is fabrication of a two-section laser cavity for picosecond pulse generation in the passive mode-locking operation mode. The key performance parameters are pulse duration of 0.5 - 10 ps, pulse repetition rate in the range of 1- 5 GHz, and average power > 10 mW.

Objective 2. Show the applicability of the UFP AAOP technology for time-resolved Raman and ultrafast spectroscopy (e.g., pump-probe technique) for specific chemical applications. For Phase I, we will demonstrate potential applications in studying the ultrafast dynamics of the photochromic reactions in diarylethene molecules.

Phase I Accomplishments

Work Plan Details of Results

Task 1: Demonstrate feasibility of AFM probe fabrication on GaAs substrate

AFM probe fabrication

Since the proposed concept of the UFP AAOP critically hinges on the ability to fabricate AFM tips from GaAs, we started processing trials during Phase I. The bulk material used was a 2" GaAs (100) wafer. AFM probes and tips are normally fabricated from silicon or silicon nitride, where the tip geometry is easily defined by the anisotropic wet-etching characteristics. For GaAs, the difference in chemical surface activity between Ga- and As-terminated planes can also lead to strongly anisotropic etching. We have tried several etchant solutions. Using a specific ratio of H_3PO_4:H_2O_2:H_2O, we were able to fabricate GaAs tips presented in Fig.2. The yield of the process was on the order of 50% and the process was found to be quite reproducible.

Fig.3 shows a GaAs AFM cantilever with the tip fabricated using wet chemical etching in an initial trial by Actoprobe. The GaAs piece is lapped to around 100 μm thick and bonded using indium to a silicon chuck taken from a commercially available AFM probe. The cantilever and tip are then formed using H_2SO_4:H_2O_2:H_2O and H_3PO_4:H_2O_2:H_2O solutions, respectively. The

cantilever has a length of 345 µm and a width of around 60 µm. The thickness of the cantilever near the tip is 8.5 µm. A tip length of 9.9 µm is achieved.

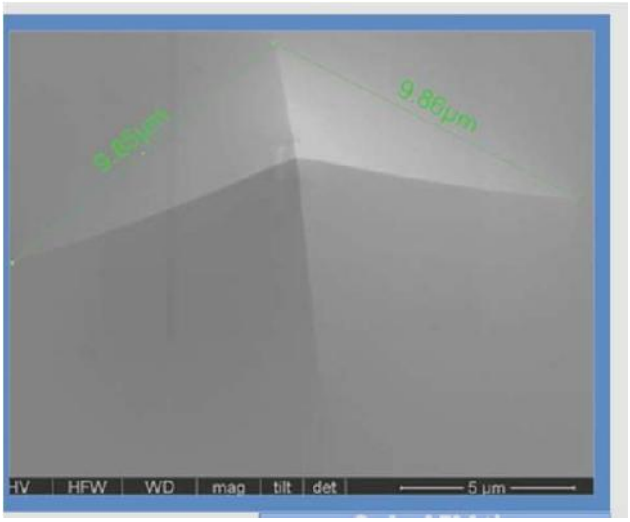

Fig.2. Top view of a GaAs tip fabricated using wet chemical etching in an initial trial by Actoprobe. The tip is tilted 25°.The tip radius achieved here is on the order of 50 nm.

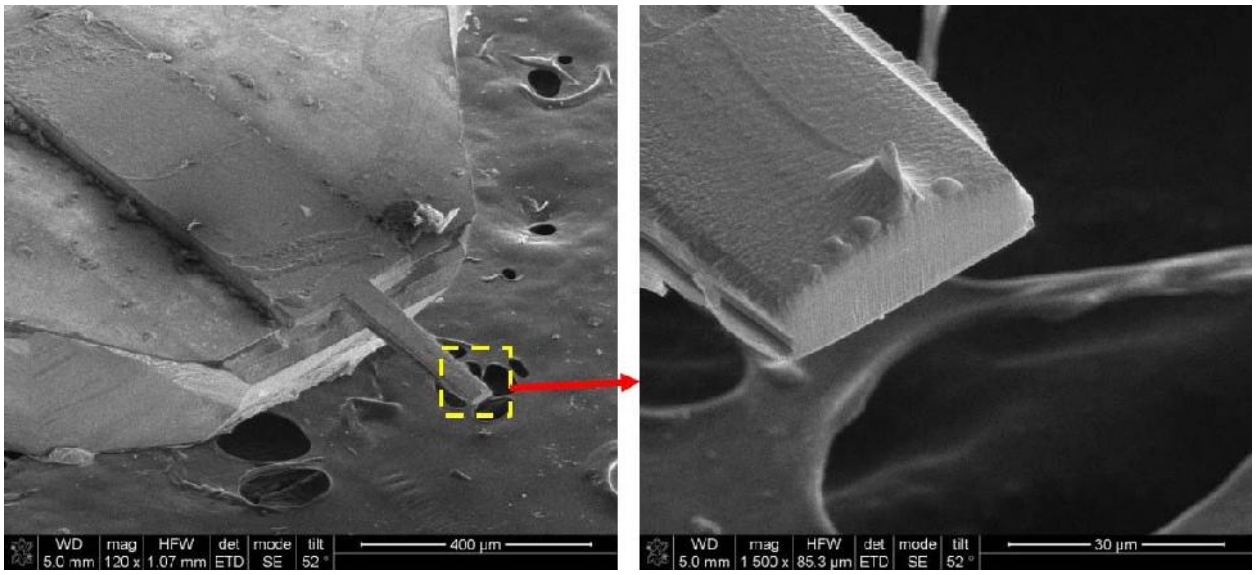

Fig.3. Left: Top view of a GaAs AFM cantilever with the tip fabricated using wet chemical etching in an initial trial by Actoprobe. Right: Close-up view of the tip. The tip length achieved here is around 9 µm.

Task 2: Test GaAs AFM probe

Since one of the UFP AAOP feasibility benchmarks is AFM resolution, we have tested the fabricated GaAs AFM probe in a conventional AFM.

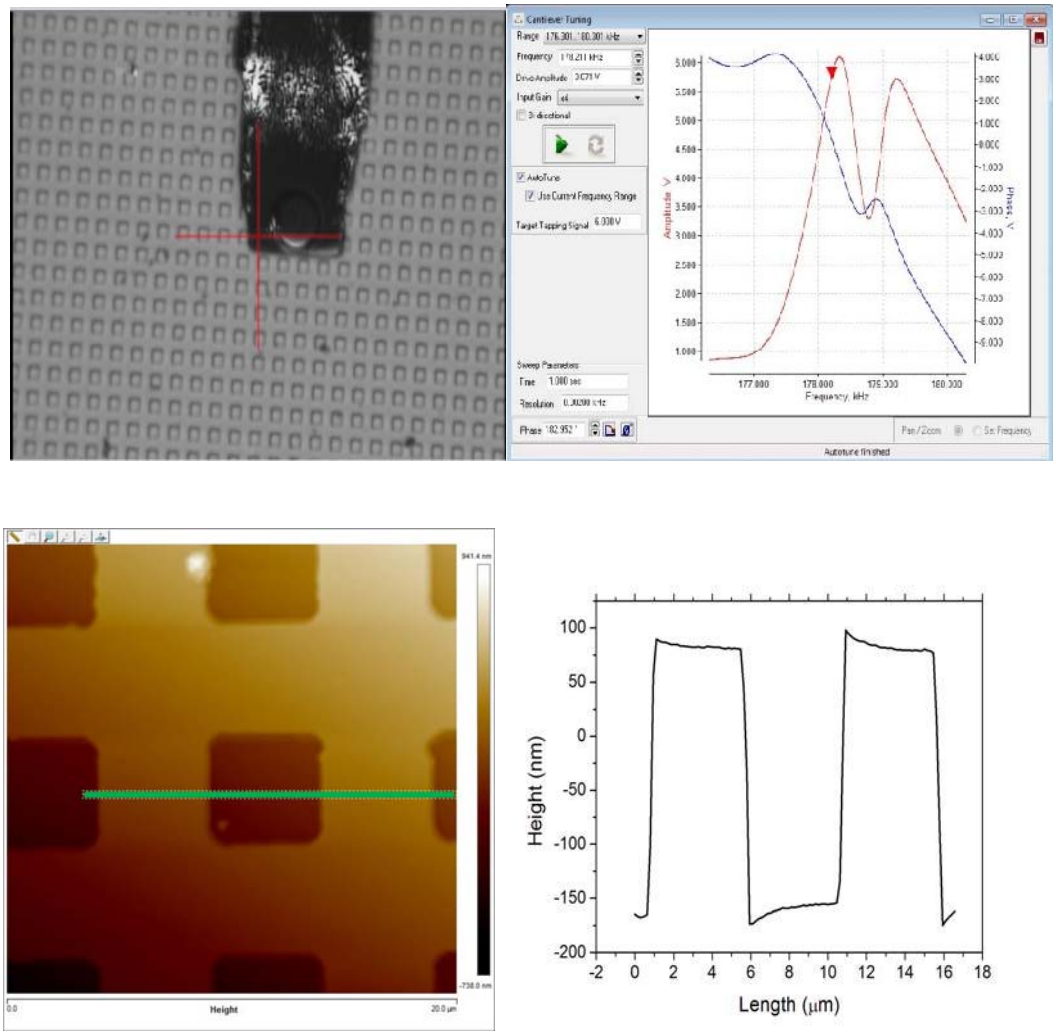

Fig.4. (Top left): The test sample and GaAs AFM tip as seen through an optical microscope. (Top right): Result of tuning the GaAs cantilever, showing a resonance frequency of around 178.5 kHz. (Bottom left): Scanned topography of the test sample using GaAs AFM.

Fig.4 shows the calibration sample (10-µm pitch, 200-nm deep) with the GaAs AFM probe as seen through an optical microscope along. A resonance frequency of around 178.5 kHz was obtained through the autotune function of the system. Also demonstrated in Fig.4 are the AFM scan results for the calibration sample, showing the topography image with the height profile across the trenches.

Task 3: Measure UFP AAOP optical resolution

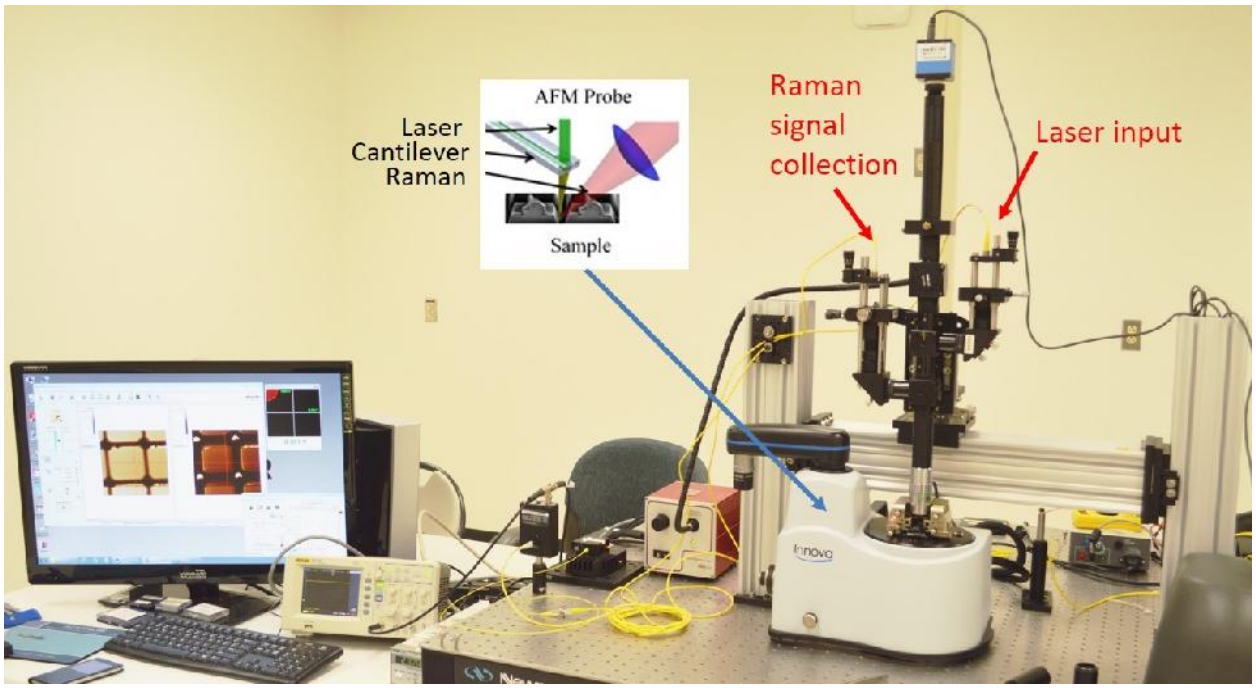

Fig.5. Experimental setup to test the probes: Bruker Innova AFM, Acto-S confocal microscope, 1.3μm laser and FW detector. Resolution: AFM - better than 20 nm; near-field - better than 20 nm; confocal - 1μm.

The UFP AAOP optical resolution was determined using the GaAs AFM probes fabricated for Task 2 (50 nm of Au was evaporated on AFM tip to optimize laser light confinement) and the Near-Field Optical Microscope setup shown in Fig.5. In this experimental setup, an external pigtail diode laser light with λ = 1.3 μm is coupled into the back of the GaAs AFM tip. This was achieved by removing the metal coating on the cantilever in a circular area exactly above the probe tip using FIB. The GaAs is transparent at 1.3 μm and the laser light propagates along the conical waveguide of the AFM tip (works as a total internal reflection conical prism) until it reaches the apex where the radiation couples into the surface plasmon mode of gold coating and focuses into a light spot a few nanometers in diameter.

The laser light enters the microscope through the laser inlet of one of the upright channels (see Fig. 5.), passes through the Au-coated AFM probe, scatters off the sample surface and is collected through the other upright channel. The signal is coupled out via single-mode fiber into a femto-watt detector (this setup also allows to couple this light into Raman spectrometer, not shown here). The camera located at the top of the center channel is used to view the sample and the AFM probe. This microscope setup can also be used with oblique laser light excitation, in this case another microscope (similar to ACTO-S confocal microscope: http://actoprobe.com/wp-content/uploads/2015/04/Isometric-view-of-Raman-AFM-setup.jpg) is installed at ~35 degrees with respect to the optical axis of the upright microscope. It is necessary to use oblique microscope when using regular AFM probes where tip apex is blocked by the cantilever and

cannot be observed with upright microscope. However, we found it much more convenient to use AFM probes of top view geometry (AFM tip apex can be observed with upright microscope: http://actoprobe.com/product/ultra-high-aspect-ratio-uhar-afm-probes-copy/#) where we applied upright excitation and upright collection and no oblique collection was necessary. Collecting the scatted near-field light vertically from the probe tip is by far more convenient and reliable than doing that at an angle (since oblique collection is bound to produce weaker signals and optical alignment is much more difficult).

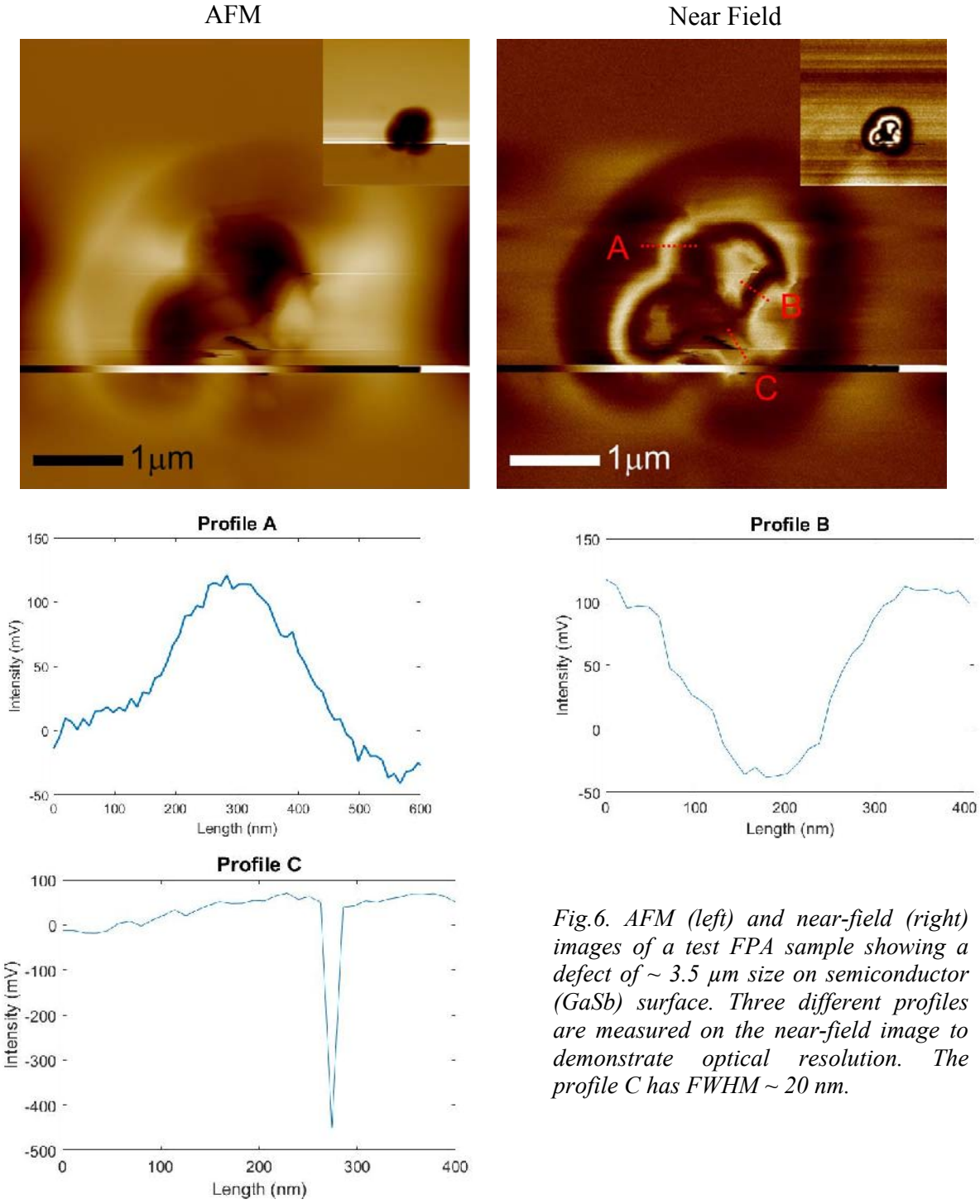

Fig.6. AFM (left) and near-field (right) images of a test FPA sample showing a defect of ~ 3.5 μm size on semiconductor (GaSb) surface. Three different profiles are measured on the near-field image to demonstrate optical resolution. The profile C has FWHM ~ 20 nm.

In Figs. 6-8 we present the near-field optical images obtained with the GaAs AFM probes fabricated for Task 2 (50 nm of Au coating on the tip) using the setup shown in Fig.5.

In Fig. 6, we present both AFM and near-field optical images of semiconductor (GaSb) surface where we can see a defect near the etching step. We can see that the near-field optical image provides additional information about the defect structure and allows us to estimate optical resolution. To do this, we measured several cross-sectional profiles on the near-field image to demonstrate that resolution can be as high as 20 nm and primarily limited by the AFM mode we used in this experiment. Indeed, in profile C, one can see a feature that has FWHM of ~ 20 nm.

In Fig. 7, we show the AFM, confocal, and near-field images of the same area of a strained layer superlattice (SLS) FPA test structure (the insets show scans of larger 85x 85 μm^2 area). It is evident that the near-field image has substantially higher resolution than the far-field confocal image of the same structure. In addition, the near-field image contains more features than the AFM and confocal ones. To compare these images in more details, we enlarged the bottom right part of each large area scan (85x85 μm^2) and showed them side by side (each image size is 35x35 μm^2). In these enlarged images, we can see even more clearly that the optical image provides additional information about the structure, as compared to the AFM and confocal ones, and the near-field image has much more superior resolution than the confocal image. In the near-field image, we can observe interesting effects, such as standing wave patterns on the deep semiconductor side walls (~ 6 μm). This laser light interference pattern is a result of interaction of the near-field optical probe with the steep side wall [18]. The AFM profile clearly shows a side-wall geometrical structure and a small oscillation pattern corresponding to the SLS layers. The confocal image profile gives us information about the reflective properties of different parts of the FPA structure. Finally, the near-field image carries information about the surface optical properties of the FPA with molecular scale resolution. When comparing the AFM and near-field images profiles, we can see that the fringe spacing depends on the side wall angle. The average fringe period is ~200 nm, which is equal to half the laser wavelength devided over the semiconductor material refractive index (~1.3 μm/2/3.5).

In Fig. 8, we present a 3D AFM image and near-field optical image of a SLS FPA showing four adjacent pixels. The AFM and near-field profiles shown are taken along the microscope scanning direction and perpendicular to the scanning direction. This FPA structure was obtained from one of the Actoprobe customer – Night Vision and Electrical Sensor Directorate (US Army). Similar to Fig. 7, the near-field optical image provides additional data about pixel side walls. We can observe here the same interference fringe pattern, which is the result of standing wave period changing with the distance between the near-field probe and the FPA side wall. It is even clearer here that the interference fringe period is in direct relation with the side wall angle. As the side wall is changing, the fringe period is changing as well. This interference pattern on the side wall can be a very advantageous feature used for mapping chemistry on side wall surfaces with tip-enhanced Raman spectroscopy. This information is very important for SLS FPA development and improvement, e.g. for finding good passivation materials for SLS FPAs. Since the fringe period is about 200 nm, which is almost hundred times smaller than the superlattice spacing, it is possible to increase Raman signal by measuring superlattice properties on the areas of the side wall where constructive interference is happening and skipping the areas where interference is destructive. In other words, we have found an additional way of focusing light on steep side wall surfaces. This will substantially improve signal to noise ratio in Raman data and will allow faster image acquisition.

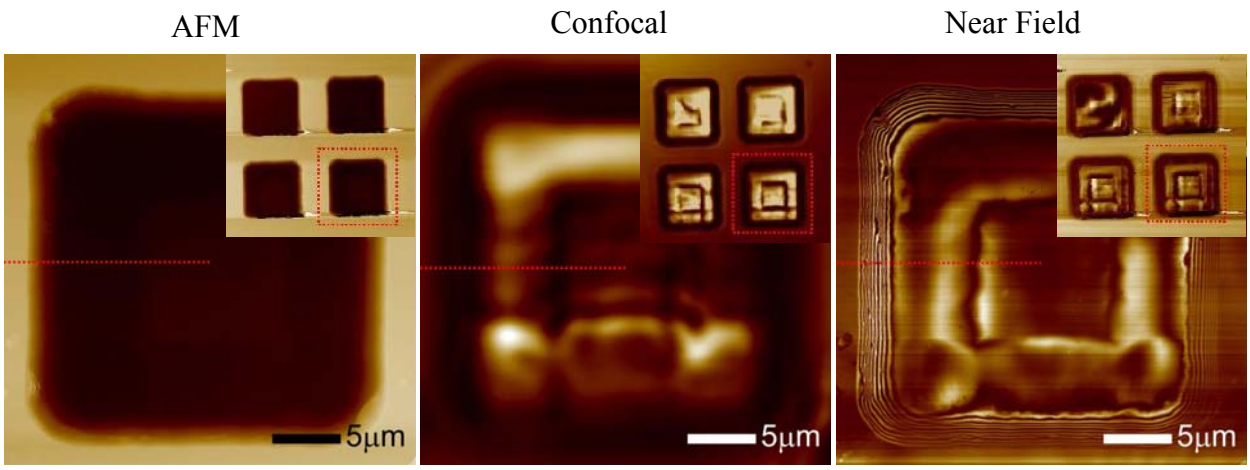

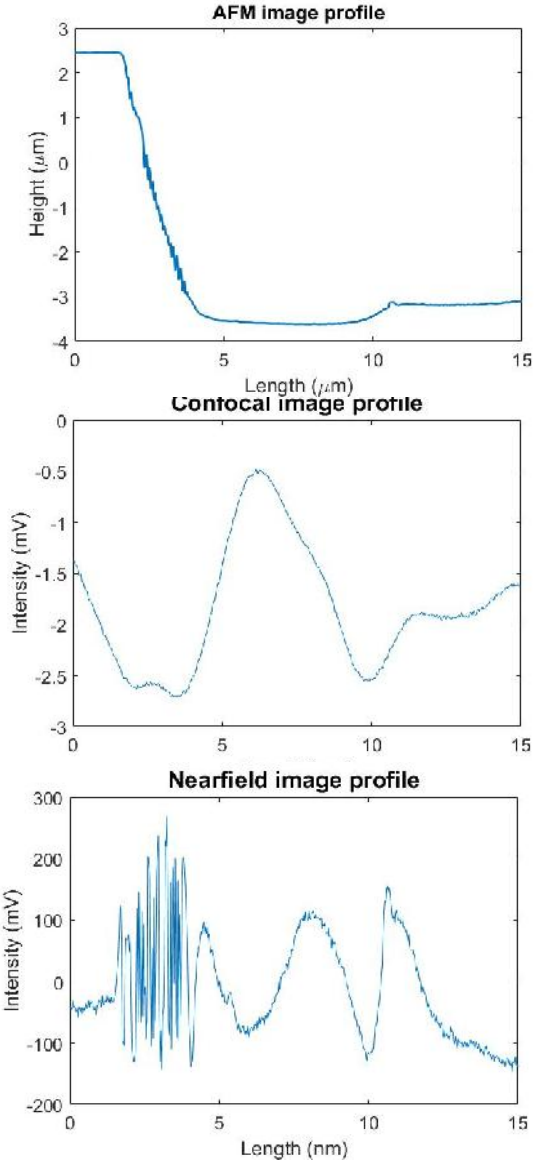

Fig.7. AFM (top left), confocal (top center) and near-field (top right) images of a focal plane array test sample. Image size is 35µm square. Insets show larger area of the test sample. Three different profiles shown below are measured on the corresponding images from the center to the edge of the images.

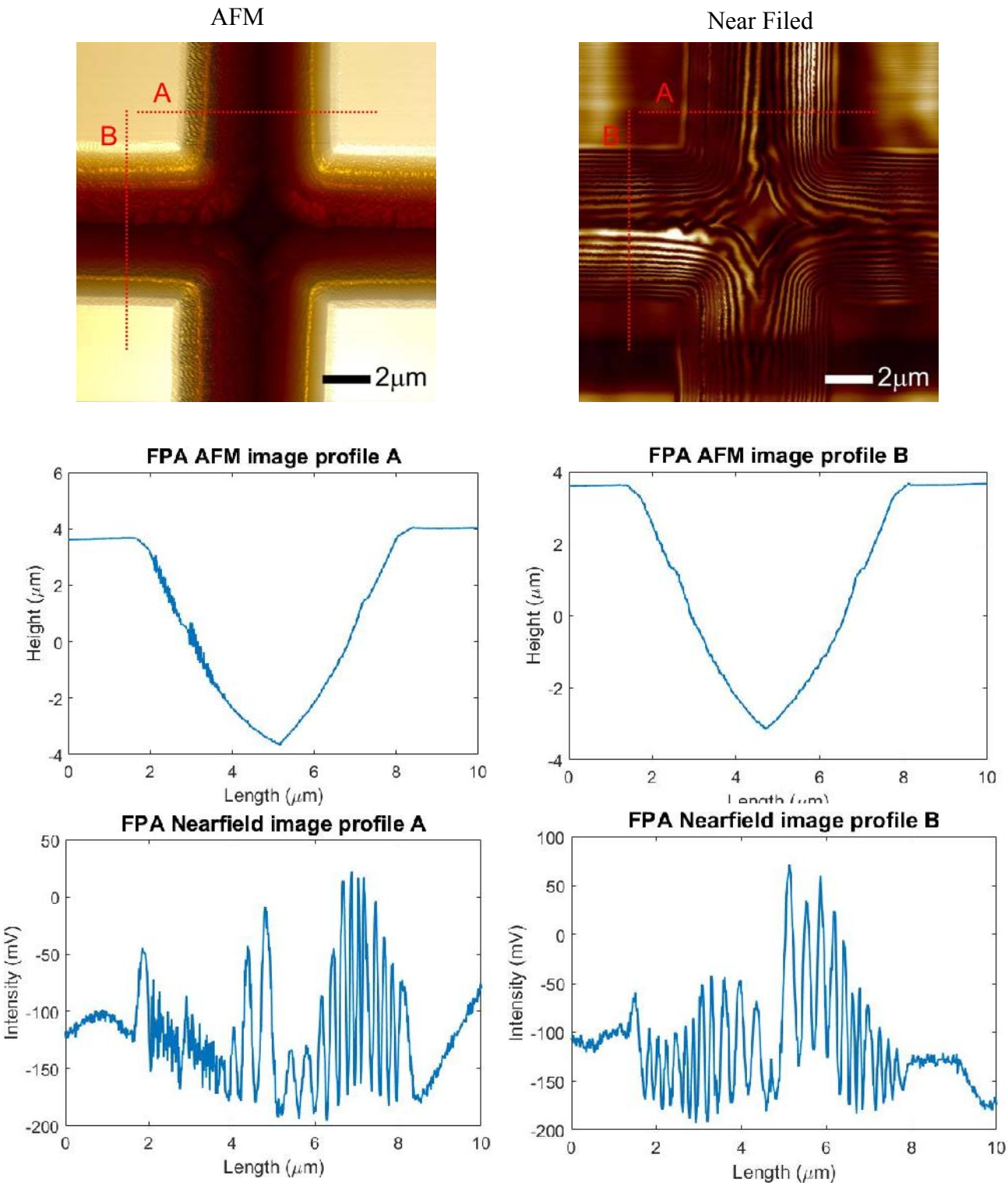

Fig.8. 3D AFM image (top left), and near-field optical image (top right) of a SLS FPA showing four adjacent pixels. AFM and near-field profiles are shown for the microscope scanning direction (A) and perpendicular to the scanning direction (B).

Task 4: Demonstrate passive mode-locking operation of two-section QD (QW) laser designed for integration with GaAs AFM probe

A two-section ridge waveguide diode laser with dimensions appropriate for integration with GaAs probe was provided by our consultant Dr. Kevin Malloy. The device was fabricated and characterized from the laser wafers according to the fabrication procedure described below. The special attention was paid to isolate the gain section from the absorber section and choose the proper voltages applied to the gain and absorber sections to achieve mode locking. The following characteristics of the passively mode-locked two-section QD laser were measured: pulse width, pulse repetition rate, optical spectrum and power spectrum. The region of stable mode locking was determined in terms of the gain section current and absorber section reverse bias.

4.1 Fabrication

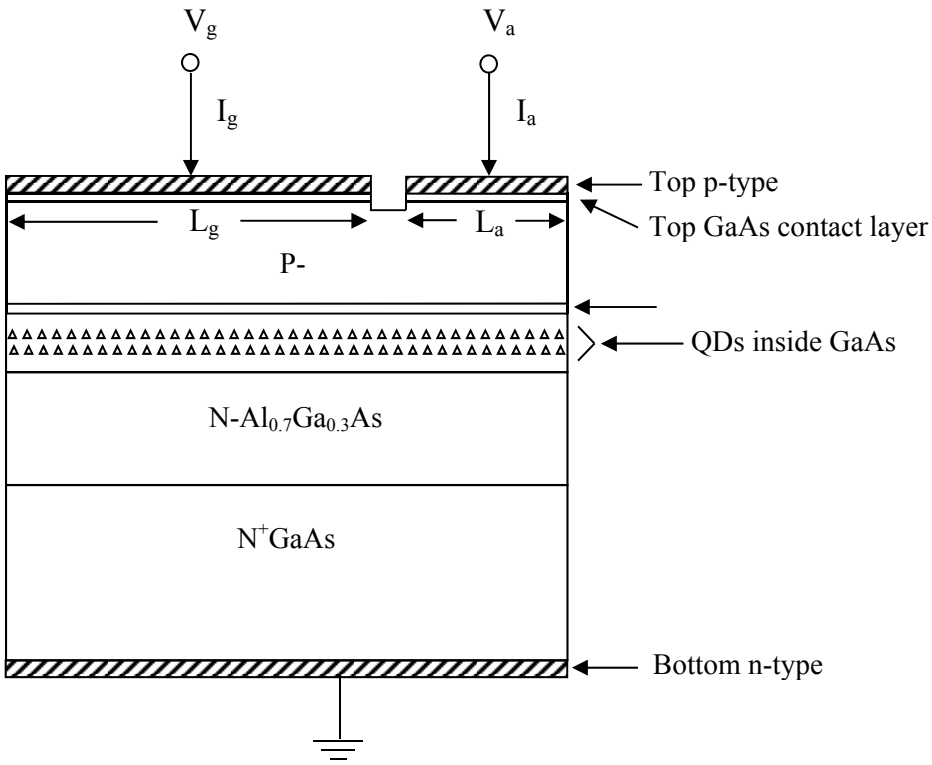

Fig.9. Schematic of the oxide-confined two-section QD laser.

The device was fabricated from a wafer grown by solid-source molecular beam epitaxy on a (001) n^+-GaAs substrate. The active region consists of two InAs quantum-dots-in-a-well layers separated by a 30 nm GaAs barrier layer, located in the middle of a 220-nm-thick GaAs waveguide bounded by $Al_{0.7}Ga_{0.3}As$ cladding layers. The device has a typical two-section laser structure with a 50 μm gap in the top p-type contact metals (Fig.9). The lengths of the gain section and the absorber section are L_g = 4.73 mm and L_a = 1.79 mm, respectively. An isolation resistance of 2.86 kΩis achieved between these two sections by using shallow dry etching to remove the heavily doped cap layer in the gap region. Current confinement is provided by the wet lateral oxidation of a 50-nm-thick $Al_{0.98}Ga_{0.02}As$ layer positioned between the waveguide and the upper cladding layers, resulting in a narrow current aperture of 10 μm. No coating was

applied to the cleaved facets. The device was mounted on a copper heat sink with the p-side up, and was tested at room temperature.

4.2 Characterization

The dc characteristics of the device were measured with current injection into the gain section (I_g) and a constant reverse bias voltage (V_a) applied to the absorber section. Room temperature lasing occurred on the QD ground state (λ=1278 nm). Fig.10 shows the output power (L) emitted from the absorber facet and the voltage (V_g) across the gain section versus the laser current under two different absorber bias conditions: (a) short-circuited, V_a= 0.0 V and (b) a reverse bias of V_a = -3.0 V. The $L - I_g$ characteristics exhibit clear counterclockwise hysteresis loops and bistability. The loop position shifts to higher laser current with increasing absorber reverse bias, while the loop width increases. We note that the V_g– I_g characteristic for V_a = -3.0 V is slightly displaced due to the leakage current between the gain section and the absorber section. Hysteresis and bistability were also observed upon applying a constant laser injection current and varying the reverse bias voltage on the absorber. The origin of bistable operation is related to the nonlinear saturation of the QD absorption occurring due to state filling and the electroabsorption originating from the quantum confined Stark effect under the applied electrical field.

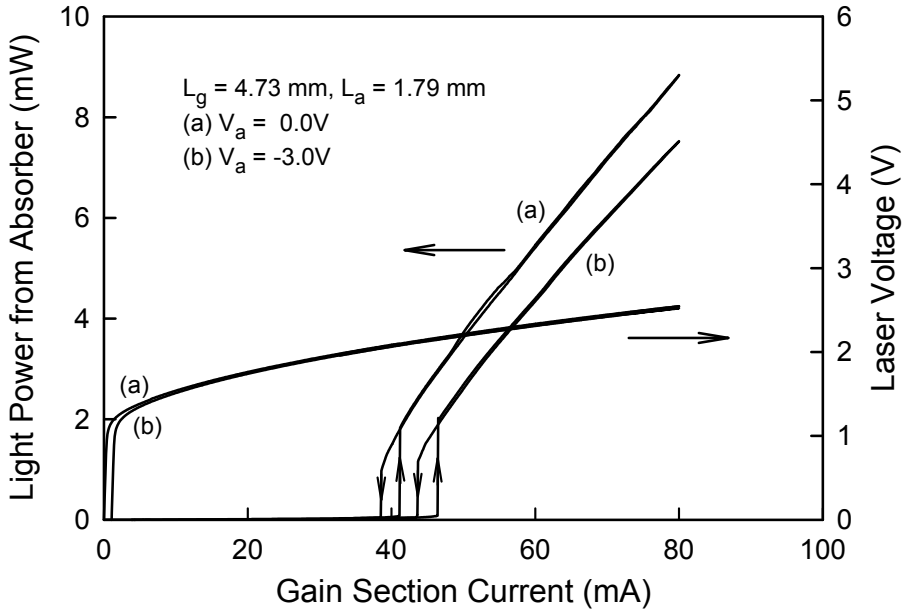

Fig.10. Room temperature lasing and electrical characteristics of a two-section QD laser under (a) an absorber short circuit with V_a = 0.0 V, and (b) a reverse bias of V_a = -3.0 V, applied to the absorber section.

Passive mode locking at a repetition rate of 7.4 GHz was achieved when both the gain and absorber sections of the lasers were dc biased. The mode-locking pulsewidth was characterized by collinear second harmonic generation intensity measured by using an autocorrelator. The narrowest mode-locked pulse was observed for absorber reverse biases between -5.0 and -6.0 V. Fig.11 shows the normalized autocorrelation traces for different gain section currents at an absorber bias of V_a = -5.0 V. A fully mode-locked pulse (giving an autocorrelation signal with a peak-to-background ratio of 3:1) was obtained for gain section current very close to the lower hysteresis threshold, I_g = 52 mA. The corresponding pulsewidth was about 17 ps, assuming a hyperbolic secant-squared pulse. As the gain section current increased, the modulation depth of the mode-locked pulse decreased and the pulsewidth quickly broadened. The closer the bias current in gain section was to the lower hysteresis threshold, the narrower the mode-locked pulse was.

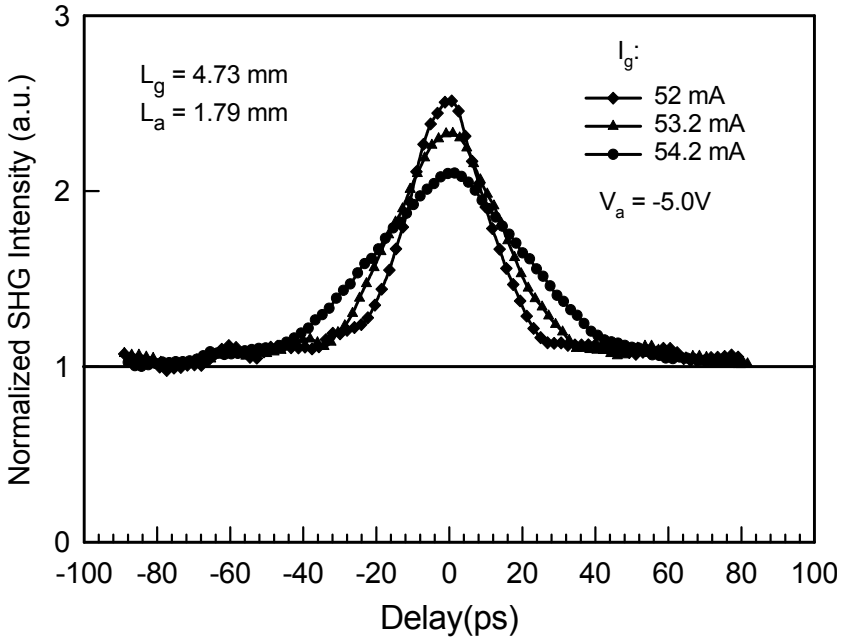

Fig.11. The normalized intensity autocorrelation traces for different gain section currents at an absorber bias of V_a = -5.0 V.

The region of mode locking and the region of bistability are shown on the I_g–V_a plot in Fig.12.Bistability occurs between the lower lasing threshold and the upper lasing threshold. The mode-locking region is bounded by the lower lasing threshold and the upper limit of measurable mode locking and overlaps with the whole bistability region. Mode locking occurs for absorber reverse biases from V_a = -6.0 V to V_a = 0.0 V, but occurs only for a relatively narrow region of gain section currents.

To measure the time-averaged optical spectrum, the output of the mode-locked QD laser was coupled into a single mode fiber and measured by an optical spectrum analyzer. Fig.13 shows that the optical spectral bandwidth of the mode-locked QD laser, under optimum bias conditions of I_g = 52 mA and V_a = -5.0 V, is about 1.07 nm corresponding to a time-bandwidth product of ~3.1, more than six times of the Fourier transform limit. This suggests the presence of phase modulation or pulse chirp.

The power spectrum of the mode-locked QD laser under the optimum bias condition of I_g = 52 mA and V_a = -5.0 V was also measured with a high-speed photodetector followed by microwave amplifiers and a rf spectrum analyzer. Two harmonics appeared in the range of 0–20 GHz, as shown in Fig.14. No self-pulsation was observed. The inset reveals the detail of the fundamental signal with a peak position at 7.4035 GHz and a 3 dB width of about 370 KHz.

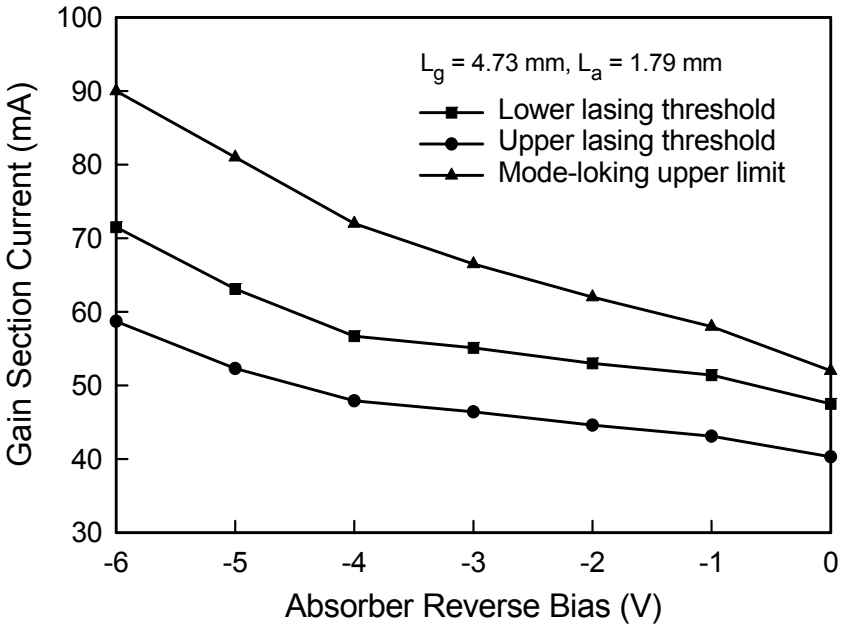

Fig.12.The mode-locking region and bistabilityregion. The region between the lower lasing threshold and the upper lasing threshold is the region of bistability. The mode-locking region extends from the lower lasing threshold to the upper limit of measurable mode locking.

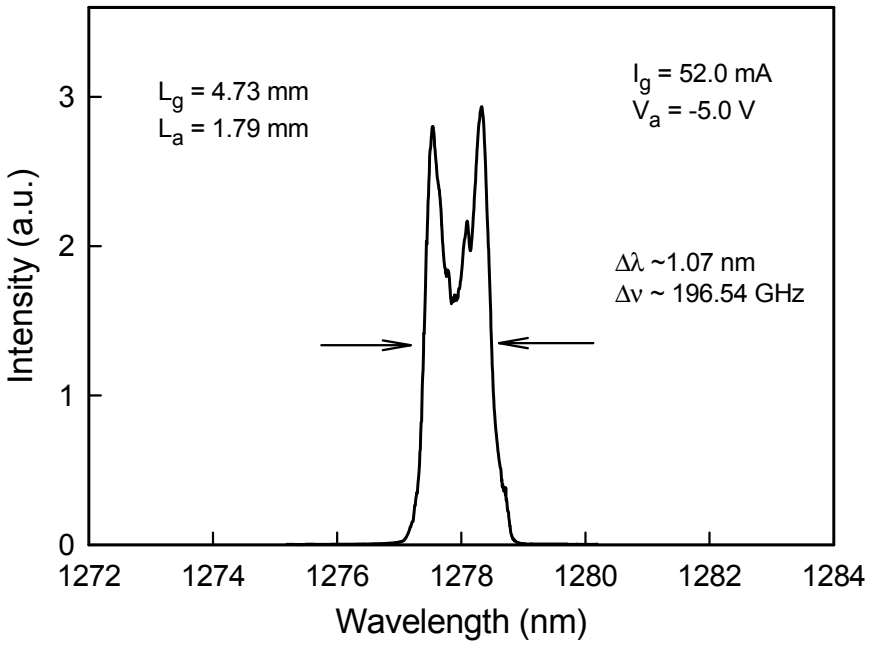

Fig.13. The optical spectrum of the mode-locked QD laser under the optimum bias condition of I_g = 52 mA and V_a = -5.0 V. The optical bandwidth is about 1.07 nm.

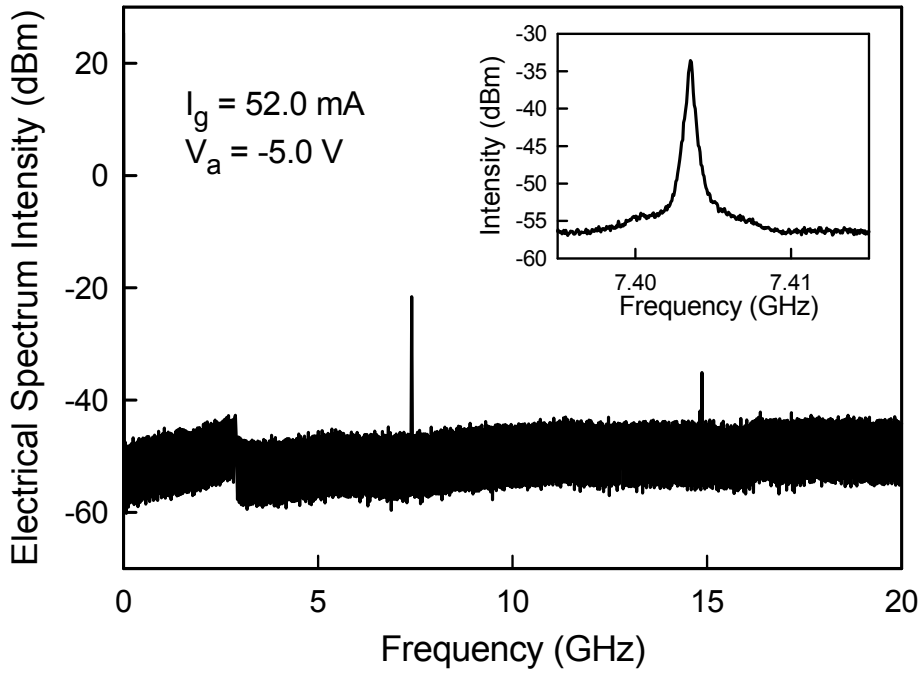

Fig.14. The power spectrum of the mode-locked QD laser under the optimum bias condition of I_g = 52 mA and V_a = -5.0 V. No self-pulsation was observed.

In conclusion, passive mode-locking operation has been demonstrated in long-wavelength, oxide-confined, two-section QD lasers designed for integration with GaAs AFM probe. Fully mode-locked pulses at a repetition rate of 7.4 GHz with duration of about 17 ps have been achieved under appropriate bias conditions. No self-pulsation has been observed accompanying the mode locking.

Task 5: Integrate monolithically a mode-locked diode laser and AFM optical probe into a single device – UFP AAOP

UFP AAOP fabrication procedure

The Actoprobe R&D team has developed a proprietary procedure for UFP AAOP fabrication from an epitaxially grown laser wafer by applying various etching techniques. The grown epitaxial laser structure consists of a double heterostructure, where the active region is placed in the core of the waveguide, sandwiched between the upper and lower cladding layers. (See Fig. 15)

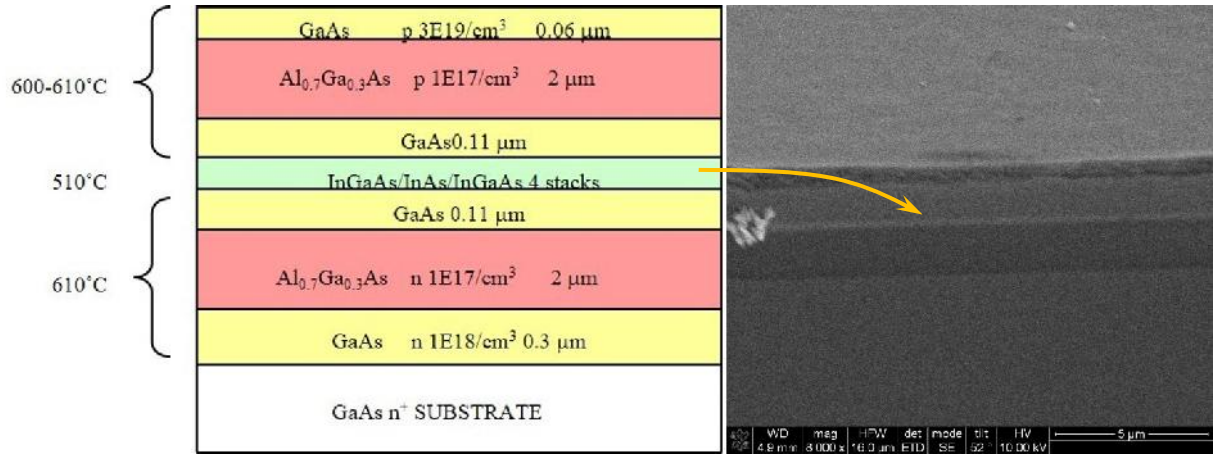

Fig.15. Epitaxial laser structure for two-section quantum dot laser.

We have succeeded in fabricating GaAs AFM cantilevers mounted on Si chucks compatible with conventional AFM holders. The obtained GaAs cantilevers are ridge-waveguide laser structures having cantilever shape with AFM tips formed at the end.

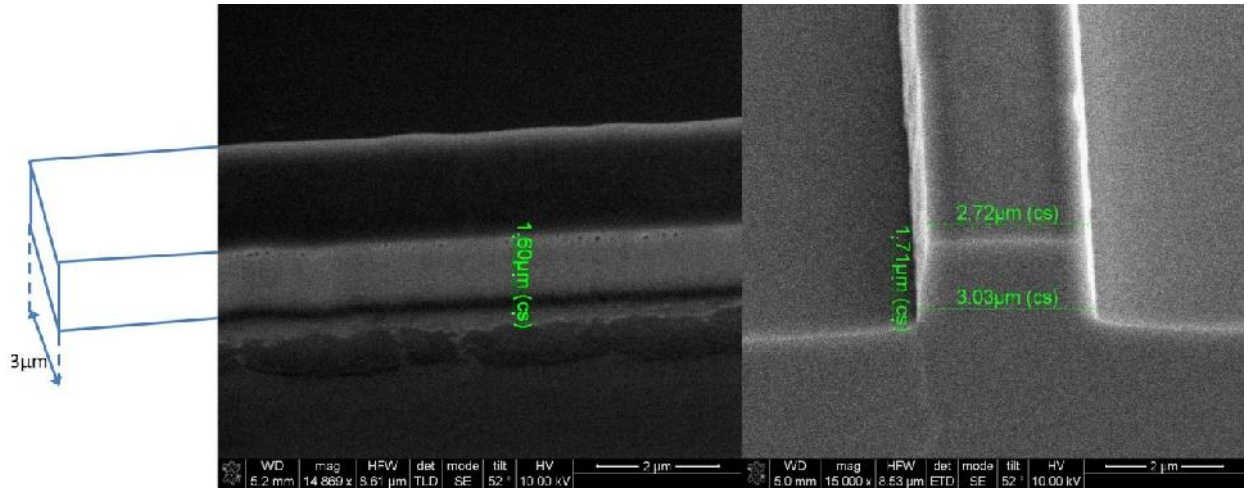

Fig.16. SEM image of GaAs ridge waveguide.

Fig. 16 illustrates a ridge waveguide laser structure obtained by patterning the wafer and etching a ridge into the upper cladding, that defines the laser cavity horizontally. Fig. 17 shows the processing step after patterning and etching the GaAs wafer into shapes of cantilevers and for separation of the devices. The shaped cantilevers incorporate ridge waveguide laser structures formed at the previous processing steps. Fig. 18 shows the GaAs AFM tips etched at the ends of the cantilevers.

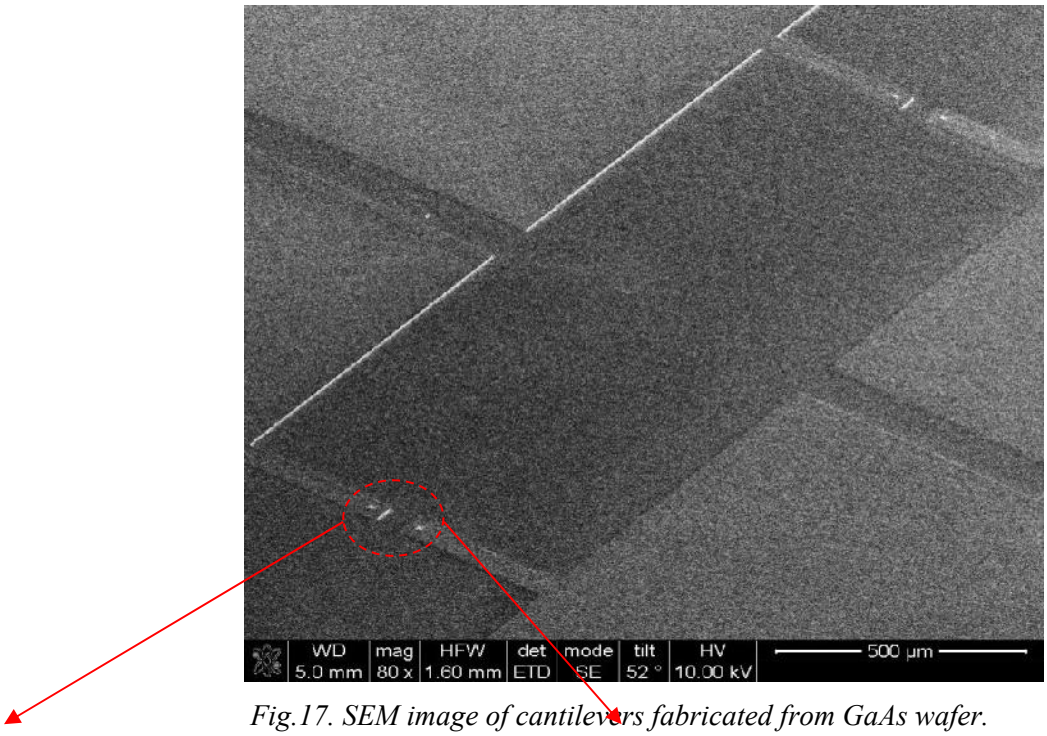

Fig.17. SEM image of cantilevers fabricated from GaAs wafer.

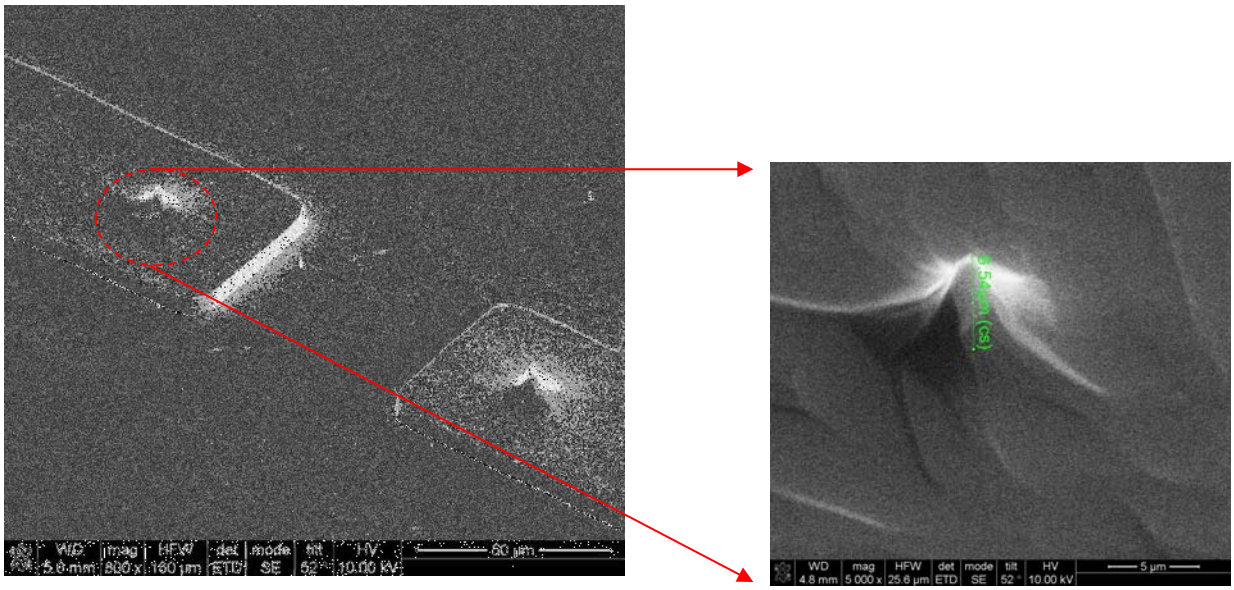

Fig.18. SEM images of the etched GaAs tips.

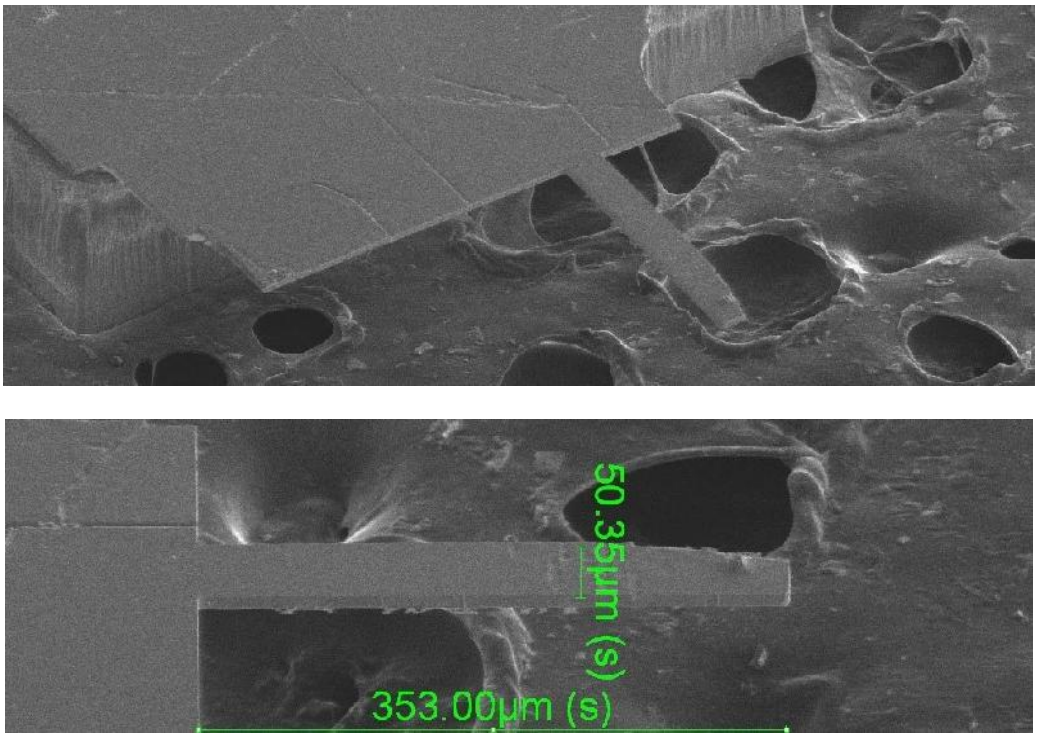

Fig.19. SEM images of prototype UFP AAOP device.

The separated GaAs cantilevers mounted on a Si chuck are shown in Fig. 19. Thus obtained prototypes of UFP AAOP devices are the ridge-waveguide laser structures having cantilever shape with AFM tips formed at the end.

In order to direct the laser light into the probe tip, it has to be deflected by 90°. The most straightforward way to accomplish that is to implement a flat surface at 45° with respect to the wafer plane. That surface acts as a folding mirror, redirecting laser light from the active region plane vertically towards the laser substrate where the probe is fabricated. Fig. 20 shows a SEM image of the folding mirror fabricated at the cleaved edge of the ridge waveguide laser.

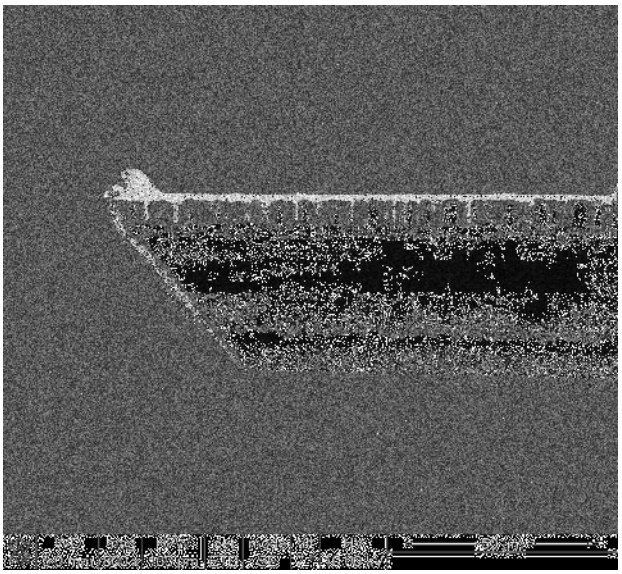

Fig.20. SEM image of the folding mirror fabricated at the cleaved edge of the ridge waveguide laser.

Task 6: Demonstrate applicability of pulsed TERS for studying the ultrafast dynamics of thephotochromic reactions in diarylethene molecules.

Preliminary characterization of the photochromic compounds

Photochromic compounds are those that change color or electronic structure when irradiated or exposed to light. This change in electronic structure is almost always accompanied by a change in molecular structure.

The photochromic compounds were provided by our consultant Dr. J. Rack, who has created a class of transition metal photochromic compounds where the mode of action (change in electronic and molecular structure) is ascribed to an excited state isomerization of a bonded sulfoxide ligand. In this family of compounds, the ground state thermodynamic isomer is an S-bonded isomer and the metastable isomer on the ground state potential energy surface is an O-bonded isomer. These photochromic ruthenium and osmium sulfoxide complexes also comprise polypyridine ligands. Their color is associated with a MLCT (Metal-to-Ligand Charge Transfer) transition from the metal dπ orbitals to the polypyridine π* orbitals. The significant covalency of the Ru–S bond coupled with the differential bonding characteristics of S- and O-bonded sulfoxides leads to the dramatic color changes observed in these complexes.

Molecular shape changes associated with photochromic action have been observed by atomic force microscopy (AFM) techniques. Shown below in Fig.21 are AFM images of the surface of a single crystal of [Ru(pic)2(dmso)2], where pic is 2-picolinate and dmso is dimethylsulfoxide.

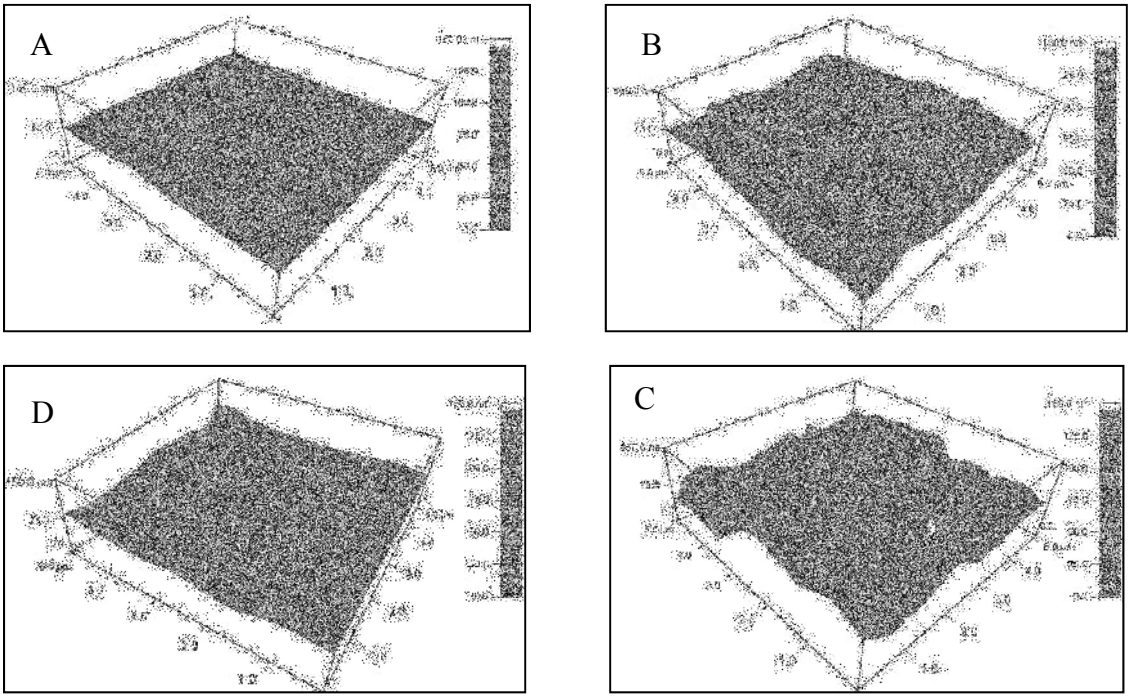

Fig.21. AFM images of the surface of a single crystal of [Ru(pic)2(dmso)2].

Panel A shows the surface of the crystal prior to irradiation with blue light (400nm). Panel B and Panel C show the same area after irradiation with 400 nm light for a period of 10 and 25 minutes. It is manifest that large distortions and demonstrable periodic changes occur on the surface of the crystal following irradiation. Panel D shows the same spot after the crystal has sat in the dark for a period of 14 hours. These data show that single crystals can feature large distortions associated with isomerization of bonded sulfoxide ligands.

More relevant to the proposed work are time-resolved transient absorption measurements of photochromic action in these compounds. Employing ultrafast pump-probe techniques, it has been observed that photo-triggered S-to-O isomerization of the sulfoxidein solution occurs on a picosecond timescale. The reaction is efficient, with typical quantum yields ranging from 0.1 to 0.9 for this class of compounds. Shown in Fig.22 are transient spectra obtained at different pump-probe time delays for a representative compound, $[Ru(bpy)_2(OSO)](PF_6)$, where bpy is 2,2'-bipyridine, and OSO is 2-methylsulfinylbenzoate, as well as the ground state absorption spectra for the S- and O-bonded isomers. From these data, it is evident that the O-bonded ground state can be formed following excitation of the S-bonded isomer with a time constant of 125 ps.

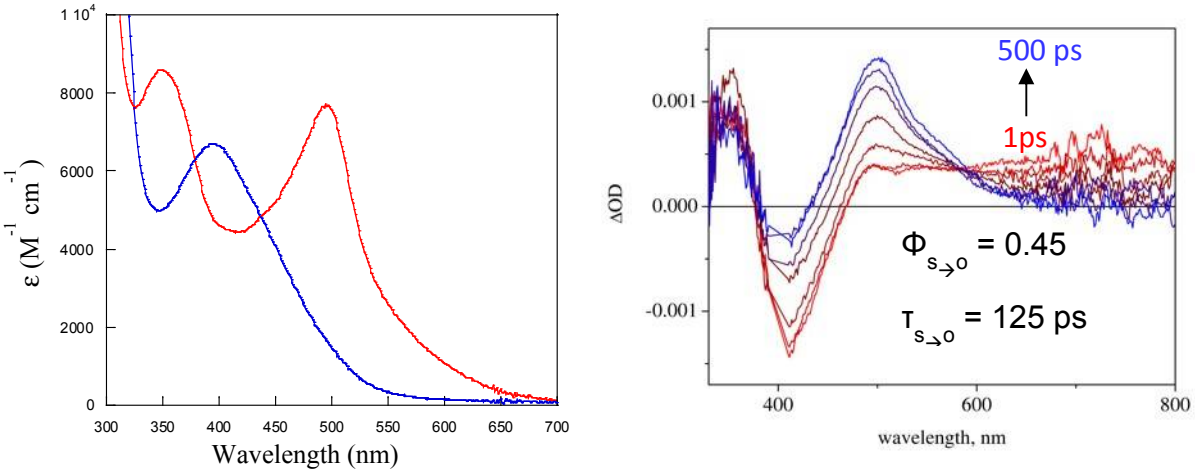

Fig.22. The ground state absorption spectra for the S- and O-bonded isomers (left), and transient spectra obtained at different pump-probe time delays for a representative compound $[Ru(bpy)_2(OSO)](PF_6)$.

These data show that the isomerization in solution occurs on rapid timescale consistent with the pulse repetition rate observed in the passively mode-locked two-section diode lasers (See section for Task 4).

We have also demonstrated the possibility to distinguish the S-bonded and O-bonded isomers in Raman spectroscopy measurements. The green curve in Fig.23 shows experimental Raman spectra of the S-bonded isomer of $[Ru(bpy)_2(OSO)](PF_6)$ tablet sample made from powder, excited with laser line at 514.5 nm. The spectrum displays vibrational band pattern as expected for Raman spectra obtained under off molecular resonance conditions. The Raman spectra of O-bonded isomer of $[Ru(bpy)_2(OSO)](PF_6)$, excited at 514.5nm, obtained after blue light (476 nm) irradiation are shown in the red curve in Fig.23. After the 405 nm laser irradiation, the color of

the compound turned from yellow transparent to dark blue and new Raman lines appeared mainly at 1550, and 1600 cm^{-1} as indicated in Fig.23. Thus, these Raman spectral changes indicate photoisomerization from S-bonded isomers into O-bonded isomers upon the 476 nm laser irradiation.

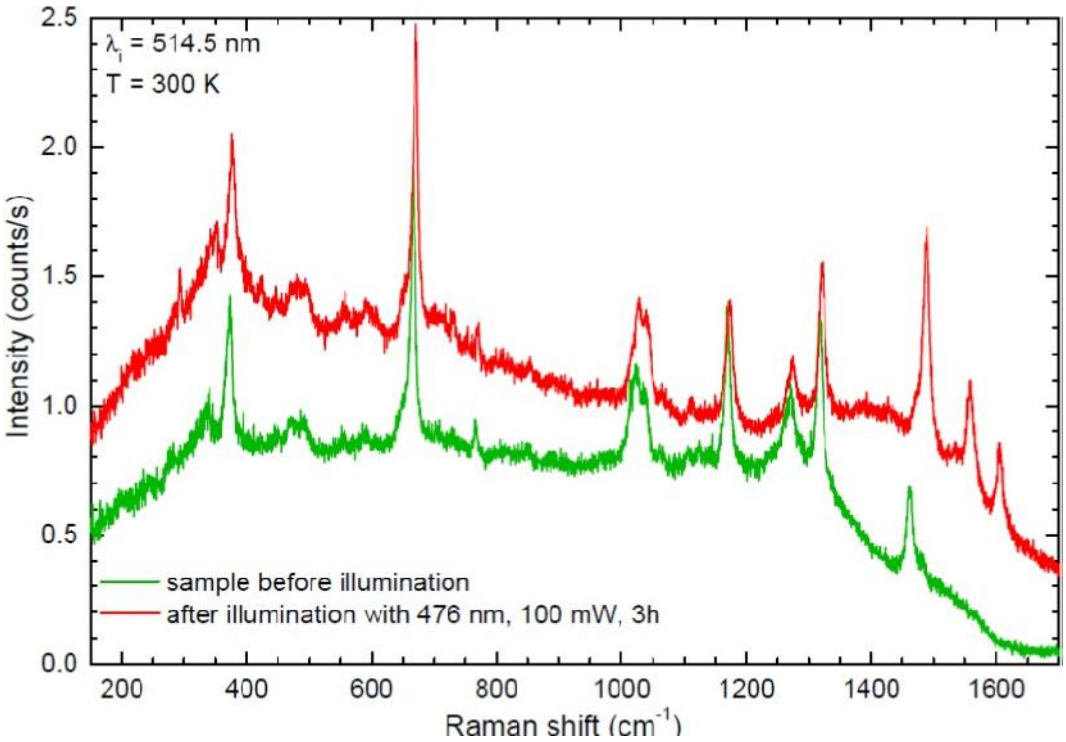

Fig.23. Raman spectra of $[Ru(bpy)_2(OSO)](PF_6)$ powder excited at 514.5 nm before and after blue laser irradiations: (green) S-bonded isomer before the 476 nm irradiation, (red) after the 405 nm irradiation.

In aggregate, the photochromic compounds provided by Dr. J. Rack are very suitable samples to test the tip-enhanced and pulsed TERS capabilities of UFP AAOP being developed by Actoprobe.

Task 7: Determine economic feasibility of UFP AAOP

During the Phase I project, in order to estimate economic feasibility of UFP AAOP, we performed marketing research by personally contacting more than 60 potential customers. Initially, we expected that our customers will be from the following three segments: 1) academic AFM users; 2) data storage companies (computer hard drive industry); and 3) CMOS imaging sensor companies. The feedback we obtained indicated that the academic AFM user segment is too small and the data storage segment is limited to just a few big players and is hard to penetrate. We found that the most attractive customer segment is companies producing CMOS imaging sensors, in particular, companies specializing in infrared military equipment. The value proposition for our technology is better performance for near-field optical microscopy, which

includes its user friendliness (similar to conventional AFM), outstanding lateral optical resolution on single molecular level (5 – 20 nm), and capability of time-resolved Raman spectroscopy on the nanoscale (AAOP output power 1 – 10 mW). We realized that for successful UFP AAOP commercialization we need to set up partnership with the existing AFM probe manufactures and distributors, such as Brucker, NT-MDT, Asylum Research, etc. We expect that our revenue streams will come from licensing the AAOP technology, AAOP sales, sales of the confocal Raman AFMs equipped with AAOP, and technical support. We are also strongly investigating the possibility to license our AAOP technology to the above-mentioned AFM companies and data storage companies (Optical Interconnects companies will also be considered).

Fabrication costs

Table 1 shows our estimates of the expected fabrication costs per probe for a small volume production of two kinds of probes: the UFP AAOP we have fabricated during this Phase I project – "Feasibility AAOP" and the newly developed design, which is scalable for high volume manufacturing – "Scalable AAOP". The initial sales price for both are expected to be roughly four times higher than fabrication costs to incorporate the other costs of manufacturing, such as R&D, marketing, and G&A.

Our implemented design in Phase I (Feasibility UFP AAOP), based on hybridization of GaAs diode laser and Si AFM chuck, allowed the development of an active optical probe prototype for application with an internal Raman laser for a reasonable cost of ~ $17,500 (see Table1) from a 2" GaAs wafer. Significant reduction in cost will be achieved by increasing production volume and using the scalable design. Applying our new UFP AAOP design (fabrication procedure) – "Scalable UFP AAOP" - invented during this Phase I SBIR (US patent pending), Actoprobe team will be able to fabricate more than 100 probes from a single 2" wafer, achieving fabrication cost of about $150 per UFP AAOP. The fabrication cost will drop tremendously with high volume manufacturing from a large number of 3" wafers processed simultaneously. We expect that pricing of well below $100 per probe will be realized.

The major difference between "Scalable UFP AAOP" and "Feasibility UFP AAOP" is that the first one does not use complicated and expansive hybridization - both the diode laser and AFM chuck are fabricated from the same GaAs chip.

Scalable UFP AAOP			Feasibility UFP AAOP		
Scenario	1 probe	100 probes	100 probes	1 probe	Scenario
Epitaxial wafer structure	$10,000	$10,000	$10,000	$10,000	Epitaxial wafer structure
Opt. Lithography + e-beam	$1,500	$1,800	$2,000	$2,000	Opt. Lithography + e-beam
Metal deposition	$500	$500	$1,000	$1,000	Metal deposition
Etching	$1,000	$1,500	$1,500	$1,500	Etching
FIB milling	-	-	$350,00	$3,500	FIB milling
Yield	90%	95%	75%	65%	Yield
Testing, packaging, other	$500	$1,000	$5,500	$2,500	Testing, packaging, other
Total cost	$13,500	$14,800	$370,000	$17,500	Total cost
Fabrication cost per probe	$15,000	**~$156**	~$47,000	$26,900	**Fabrication cost per probe**
Sale price estimate (x2)	$30,000	**$312**	$94,000	$53,846	**Sale price estimate (x2)**

Table 1. Estimates of probe fabrication costs for two UFP AAOP designs (fabrication procedures): "Feasibility" and "Scalable" and for two different scenarios: i) single probe fabrication and ii) fabrication of 100 probes. Processing costs are based on estimates of required time and appropriate tool, supply, and operator costs. The conservative cost estimate given is obtained by multiplying the estimated cost per probe by a safety factor of 2.

Task 8: Analyze scale up manufacturing potential and expected manufacturing speed

UFP AAOP has a large potential for high volume production due to Actoprobe team invention of the "Scalable" probe design and fabrication procedure (see above).

Manufactured speed is primarily limited by the following fabrication procedures:

1. MBE growth of the QD laser structure takes up to 10 hours (up to 8 3" GaAs wafers simultaneously grown using larger industrial MBE machines)
2. Clean room processing would take up to 24 hours using high volume manufacturing facilities: lithography, thermal and metal evaporation, etching, etc.
3. Testing and packaging takes up to 8 hours with automatic test stations

About 225 probes will come out of each of 3" wafers resulting in 1800 probes for 42 hours of manufacturing time, i.e. about 43 probes per hour. This manufacturing speed will allow us to fabricate up to ~ 100,000 UFP AAOPs per year with revenue more than $30,000,000 assuming sale price of each probe $312 as shown in Table1.

Conclusions

The overall objective of the Phase I SBIR project was to demonstrate the technical feasibility of a novel class of probes for atomic force microscopy – Ultrafast Pulsed Active AFM Optical Probe that will enhance characterization capabilities at the nanoscale. This probe, providing ultrafast pulsed optical excitation together with atomic force microscopy, will revolutionize the technique of tip-enhanced Raman spectroscopy for non-destructive time-resolved morphological and chemical characterization of the sample at the nanoscale.

As a result of the Phase I project, we have demonstrated the feasibility of UFP AAOP concept. We have successfully fabricated active optical AFM probe that incorporate passive mode-locked GaAs-based diode laser and GaAs AFM probe. Excellent performance of the probe has been proved in terms of AFM and optical spatial resolution through rigorous tests. The observed 20-nm optical resolution implies the potential capability for the probe to characterize chemical compounds with single-molecule resolution. Unique spatial information has been obtained from the near-field images, which implies very interesting potential applications of the probe for IR sensor characterization and development. Time-resolved capability of the probe has been provided by passive mode-locking operation of a two-section laser structure integrated into the probe. We have shown that passive mode-locking operation provides short optical pulses at a repetition rate of 7.4 GHz with duration of ~17 ps, which makes it very attractive for time-resolved optical spectroscopy. The UFP AAOP fabrication procedure has been developed for wafer scale production of multiple devices, with the yield of the process estimated to be ~90%.

We have identified the particular photochromic compounds to be very good candidates for future testing of UFP AAOP time-resolved capability (pulsed TERS). We have demonstrated the applicability of Raman for studying the dynamics of photochromic reactions in diarylethene molecules by showing the differences in Raman spectra recorded before and after isomerization. UFP AAOP is expected to ensure single-molecule resolution for such measurements. Finally, economic feasibility and scale-up manufacturing potential was analyzed for UFP AAOP and found to be very encouraging.

In summary, the Actoprobe team has successfully accomplished all of its Phase I tasks and demonstrated the feasibility of the UFP AAOP concept. We believe that this success provides a strong foundation for the Phase II project, for which the main objective will be further development and small volume production of UFP AAOP.

References

[1] C. C. Neacsu, S. Berweger and M. B. Raschke, "Tip-Enhanced Raman Imaging and Nanospectroscopy: Sensitivity, Symmetry, and Selection Rules," *NanoBiotechnology,* vol. 3, no. 3, pp. 172-196, 2007.

[2] M. Celebrano, P. Biagioni, M. Zavelani-Rossi, D. Polli, M. Labardi, M. Allegrini, M. Finazzi, L. Du`o and G. Cerullo, "Hollow-pyramid based scanning near-field optical microscope coupled to femtosecond pulses: A tool for nonlinear optics at the nanoscale," *Review of Scientific Instruments,* vol. 80, no. 3, p. 033704, 2009.

[3] J. W. Kingsley, S. K. Ray, A. M. Adawi, G. J. Leggett and D. G. Lidzey, "Optical nanolithography using a scanning near-field probe with an integrated light source," *Appl. Phys. Lett.,* vol. 93, no. 21, p. 213103, 2008.

[4] K. Hoshino, A. Gopal and X. Zhang, "Near-field scanning nanophotonic microscopy – breaking the diffraction limit using integrated nano light-emitting probe tip," *IEEE Journal of Selected Topics in Quantum Electronics,* vol. 15, no. 5, pp. 1393-1399, 2009.

[5] K. H. An, B. O'Connor, K. P. Pipe, Y. Zhao and M. Shtein, "Scanning probe optical microscopy using an integrated submicron organic photodetector," in *Lasers and Electro-Optics and Conference on Quantum Electronics and Laser Science*, San Jose, 2008.

[6] R. R. Frontiera, A. I. Henry, N. L. Gruenke and R. P. V. Duyne, "Surface-Enhanced Femtosecond Stimulated Raman Spectroscopy," *J. Phys. Chem. Lett.,* vol. 2, no. 10, pp. 1199-1206, 2011.

[7] A. A. Lanin, E. A. Stepanov, R. A. Tikhonov, D. A. Sidorov-Biryukov, A. B. Fedotov and A. M. Zheltikov, "Multimodal nonlinear Raman microspectroscopy with ultrashort chirped laser pulses," *JETP Lett.,* vol. 101, no. 9, pp. 593-597, 2015.

[8] N. Everall, T. Hahn, P. Matousek, A. W. Parker and M. Towrie, "Picosecond Time-Resolved Raman Spectroscopy of Solids: Capabilities and Limitations for Fluorescence Rejection and the Influence of Diffuse Reflectance," *Applied Spectroscopy,* vol. 55, no. 12, pp. 1701-1708, 2001.

[9] I. Nissinen, J. Nissinen, P. Keranen, A. K. Lansman, J. Holma and J. Kostamovaara, "A 2 X (4) X 128 Multitime-Gated SPAD Line Detector for Pulsed Raman Spectroscopy," *IEEE Sensors Journal,* vol. 15, no. 3, pp. 1358-1365, 2015.

[10] J. M. Klingsporn, M. D. Sonntag, T. Seideman and R. P. V. Duyne, "Tip-Enhanced Raman Spectroscopy with Picosecond Pulses," *J. Phys. Chem. Lett.,* vol. 5, no. 1, pp. 106-110, 2014.

[11] M. D. Sonntag, E. A. Pozzi, N. Jiang, M. C. Hersam and R. P. V. Duyne, "Recent Advances in Tip-Enhanced Raman Spectroscopy," *J. Phys. Chem. Lett.,* vol. 5, no. 18, pp. 3125-3130, 2014.

[12] L. Novotny and N. v. Hulst, "Antennas for light," *Nature Photonics,* vol. 5, pp. 83-90, 2011.

[13] E. U. Rafailov, M. A. Cataluna and W. Sibbett, "Mode-locked quantum-dot lasers," *Nature Photonics,* vol. 1, pp. 396-401, 2007.

[14] E. U. Rafailov, M. A. Cataluna, W. Sibbett, N. D. Il'inskaya, Y. M. Zadiranov, A. E. Zhukov, V. M. Ustinov, D. A. Livshits, A. R. Kovsh and N. N. Ledentsov, "High-power picosecond and femtosecond pulse generation from a two-section mode-locked quantum-dot laser," *Appl. Phys. Lett.,* vol. 87, no. 8, p. 081107, 2005.

[15] X. Huang, A. Stintz, H. Li, L. F. Lester, J. Cheng and K. J. Malloy, "Passive mode-locking in 1.3 μm two-section InAs quantum dot lasers," *Appl. Phys. Lett.,* vol. 78, no. 19, pp. 2825-2827, 2001.

[16] X. L. Wang, H. Yokoyama and T. Shimizu, "Synchronized harmonic frequency mode-locking with laser diodes through optical pulse train injection," *IEEE Photon. Tech. Lett.,* vol. 8, no. 5, pp. 617-619, 1996.

[17] T. Virgili, G. Grancini, E. Molotokaite, I. Suarez-Lopez, S. K. Rajendran, A. Liscio, V. Palermo, G. Lanzani, D. Polliac and G. Cerulloa, "Confocal ultrafast pump-probe spectroscopy: a new technique to explore nanoscale composites," *Nanoscale,* vol. 4, no. 7, pp. 2219-2226, 2012.

[18] B. Hecht, H. Bielefeldt, Y. Inouye, D. W. Pohl, and L. Novotny, "Facts and artifacts in near-field optical microscopy", *J. Appl. Phys.*, vol. 81, no. 6, pp. 2492-2498, 1997.

Acknowledgements

This work was performed, in part, at the Center for Integrated Nanotechnologies, an Office of Science User Facility operated for the U.S. Department of Energy (DOE) Office of Science by Los Alamos National Laboratory (Contract DE-AC52-06NA25396) and Sandia National Laboratories (Contract DE-AC04-94AL85000). The Actoprobe LLC team would like to thank the faculty and technical staff of the Center for High Technology Materials (CHTM) at the University of New Mexico for fruitful discussions and technical support.